Electronic Supplementary Material (ESI) for Inorganic Chemistry Frontiers.

Supporting information

$BaMnSnS_4$ and $BaCdGeS_4$: Infrared Nonlinear Optical Sulfides Containing Highly Distorted Motifs with Centers of Moderate Electronegativity.

Yang-Jie Lin, Run Ye, Long-Qi Yang, Xiao-Ming Jiang,* Bin-Wen Liu, Hui-Yi Zeng, and Guo-Cong Guo*

State Key Laboratory of Structural Chemistry, Fujian Institute of Research on the Structure of Matter, Chinese Academy of Sciences, Fuzhou, Fujian 350002, P.R. China

CONTENTS

Figure S8. Calculated birefringence Δn of **1 (a)** and **2 (b)**.

Figure S9. (a) Variable-temperature χ_m (left) and $\chi_m T$ (right) curves of **1**. (b) Variable-temperature $1/\chi_m$ curve of **1**.

3. References

1. Experimental Section

Reagents. All of the reagents are used as received without further purification, and were operated inside an argon-filled glovebox with controlled oxygen and moisture levels of <0.1 ppm: Ba (99.0%), Mn (99.9%), Cd (99.999%), Sn (99.99%), Ge (99.99%), S (99.95%). All chemicals were bought from Aladdin Chemistry Co. Ltd. Dark red Crystals of **1** were obtained from a reaction mixture containing Ba (0.66 mmol), Mn (0.66 mmol), Sn (0.66 mmol) and S (2.65 mmol), which was loaded into quartz tubes and flame-sealed under vacuum (~1×10^{-4} Torr). The tubes were placed into a computer-controlled furnace, heated up to 250 °C and held at that temperature for 2 hours, then heated up to 875 °C in 24 hours and kept for 96 hours, and then cooled down to 300 °C at 4 °C/hour before switching off the furnace. Light green crystals of **2** were crystallized from a reaction mixture containing Ba (0.66mmol), Cd (0.66mmol), Ge (0.66mmol) and S (2.65mmol) with the same synthesis process as **1**. The product yields were approximate 80% for both **1** and **2**. They all are stable in the air and moisture condition.

Single-Crystal Structure Determination. Single crystals of title compounds were mounted on glass fibers for single-crystal XRD measurements. The diffraction data were collected using graphite-monochromated Mo−Kα radiation (λ = 0.71073 Å) on a Rigaku Pilatus diffractometer at 293 K. In which a ω-scan technique was used for the collection of intensity datasets, and the datasets were reduced using CrystalClear.[1] The structures of single crystals were solved by direct methods and refined through full-matrix least-squares techniques on F^2 with anisotropic thermal parameters for all atoms. All of the calculations were performed using the Siemens SHELXL package of crystallographic software.[2] The final structures were examined for additional symmetry with ADDSYM/PLATON[3] and no other higher symmetry was observed. The crystallographic data and structure refinement results of title compounds are given in Table S1. Atomic coordinates are listed in Table S2.

Powder X-ray Diffraction. The powder X-ray diffraction data of **1** and **2** were recorded on a Rigaku MiniFlex600 diffractometer with Cu Kα (λ = 1.54057 Å) radiation in reflection mode at room temperature with a step width of 0.02° in the 2θ range of 5-65°. The experimental results and the simulated patterns generated using the Mercury program are shown in Fig. S1, indicating

that the powder samples used for the further properties measurements are pure.

Energy-Dispersive X-ray Spectroscopy (EDS). A scanning electron microscope (FESEM, JSM6700F) equipped with energy dispersive X-ray spectroscopy (EDS, Oxford INCA) was used to do the semiquantitative element analyses of the title compounds. The empirical formulas for **1** and **2** are $Ba_{1.0}Mn_{0.9}Sn_{1.0}S_{3.8}$ and $Ba_{1.0}Cd_{0.9}Ge_{0.9}S_{3.9}$, respectively, which are consistent with the results from single-crystal structure determination.

Infrared and UV−Vis−NIR Diffuse Reflectance Spectroscopy. The Fourier transform IR spectra of title compounds were obtained by using a PerkinElmer Spectrum One FRIR spectrometer in the range of 400−4000 cm^{-1}. The powder samples were mixed with KBr to press into pellets. The optical diffuse reflectance spectra of powder samples were measured using PerkinElmer Lambda 900 UV−vis spectrometer in the range of 200−2500 nm with $BaSO_4$ as a standard for the background at room temperature. The KubelkaMunk equation[4]: $\alpha/S = (1-R)^2/2R$, (where α is the absorption coefficient, S is the scattering coefficient, and R is the reflectance) was used to calculate the absorption spectra from reflection spectra.

Thermal Analyses. The thermal properties of title compounds were carried out with differential scanning calorimetry (DSC) analyses by Mettler Toledo TGA/DSC apparatus under a nitrogen atmosphere. The powder samples with approximate 20 mg for each compound were sealed in silica tubes and then evacuated to 1×10^{-4} Torr. The tubes were heated to 1000 °C and then cooled to 30 °C at 20 °C/min (Fig. S4).

SHG Measurements. The powder SHG measurements for the title compounds were performed by using a modified Kurtz Perry powder technique with a 1910 nm laser radiation.[5] The powder samples of **1** and **2** were sieved into several discrete particle size ranges of 30−50, 50−75, 75−100, 100−150, 150−200, and 200−250 μm for the SHG phase-matching measurements. The commercial AGS powders sieved with similar particle sizes were used as the standard. The doubled frequency signals (955 nm) were measured by using an Andor DU420A-BR-DD CCD camera.

Powder LIDTs Measurements. The powder LIDTs of title compounds and the reference AGS were measured through single pulse method.[6] All the samples in the same size range (0.25-

0.30mm) were pressed into glass microscope cover slides, exposing to high-power 1064 nm laser radiation with a pulse width τp of 10 ns in a 1 Hz repetition. The principle of damage threshold determination is that a single pulse radiation was passed and gradually increasing the laser power until a damaged spot on the samples was observed. The Nova II sensor display with a PE50-DIF-C energy sensor was used to measure the power of the laser beam.

Magnetic measurements. Magnetic susceptibility of **1** was measured under an applied field of 1000 Oe from 300 to 2 K using a commercial Magnetic Property Measurement System (MPMS).

Computational Descriptions. The distortion of tetrahedral units in **1** and **2** were measured with two definitions. One is ΔH, proposed by Lalik using Shannon's information theory.[7] $\Delta H = \left(\frac{A}{V}\right)\sum_i \left[s_i \ln\left(\frac{s_i}{s'}\right)\right] = A < \left(\frac{s_i}{s'}\right) ln(\frac{s_i}{s'}) >$, where the summation is over the N bonds in the coordination polyhedron, <> indicates an average value over the coordinated bonds, A is a constant equal to 1/ln2, V is the formal oxidation state of the central cation, s_i is the valence of the ith bond and s' is the average valence of the bonds in the coordination sphere. The bond valence s_i is calculated using $s_i = \exp[(R_o\text{-}R_i)/B]$,[8] where R_o and B are empirically determined constants for each type of bond, with the former being the notional length of a bond of unit valence and the latter a measure of the softness of the bond. These parameters have been tabulated for most bond types by Brown.[9] The other one is ΔR, proposed by Brown. $\Delta R = -(BN) i \ln\frac{s_i}{s'} = -B < \ln\frac{s_i}{s'} >$, where B, N, s_i and s' have the same meanings as above.[10]

The Mulliken bond populations, electronic band structures and densities of state (DOS) of **1** and **2** were calculated using the CASTEP package.[11] The generalized gradient approximation[12] was chosen as the exchange-correlation functional, and the norm-conserving pseudo potentials[13] were used. The valence electron configurations for Ba, Mn, Cd, Ge, Sn and S were $5s^25p^66s^2$, $3d^54s^2$, $4d^{10}5s^2$, $4s^24p^2$, $5s^25p^2$ and $3s^23p^4$ respectively. The numerical integration of the Brillouin zone was performed using 3 × 3 × 3 Monkhorst−Pack κ-point meshes for both compounds. The Fermi level (E_f =0 eV) was selected as the energy reference for all the band structure and DOS presentations.

The frequency-dependent SHG susceptibility of **1** and **2** was calculated based on density functional perturbation theory using the ABINIT computer code package[14] and sum formalism of Sharma,[15] in which the SHG susceptibility can be divided into three major contributions: the interband transitions $\chi_{inter(2\omega,\ \omega,\ \omega)}$, the intraband transitions $\chi_{intra(2\omega,\ \omega,\ \omega)}$ and the modulation of interband terms by intraband terms $\chi_{mod(2\omega,\ \omega,\ \omega)}$. Refractive index n was obtained according to the formula:[16] $n(\omega) = \sqrt{\frac{\sqrt{\varepsilon_1^2(\omega) + \varepsilon_2^2(\omega)} + \varepsilon_1(\omega)}{2}}$, where $\varepsilon_1(\omega)$ and $\varepsilon_2(\omega)$ are real and imaginary parts of the dielectric function, respectively.

DFT calculations of ELF employed the projector augmented wave method encoded in the Vienna ab initio simulation package,[17] the local density approximation (LDA), and the plane wave cutoff energy of 500 eV.

2. Figures and Tables

Table S1. Crystallographic data and structure refinement results for **1** and **2.**

	1	**2**
Temperature (K)	293(2)	293(2)
Space group	*Fdd*2	*Fdd*2
a (Å)	21.547(5)	21.285(4)
b (Å)	21.796(3)	21.691(5)
c (Å)	12.981(3)	12.786(4)
V (Å^3)	6096(2)	5903(3)
Z	32	32
D_{calcd} (g cm^{-3})	3.828	4.056
μ (mm^{-1})	10.974	13.193
2θ range (deg)	5.32-55.13	6.76-50.98
GOF on F^2	0.996	1.051
R_1[a] [$I>2\sigma(I)$]	0.0346	0.0169
wR_2[b] [$I>2\sigma(I)$]	0.0808	0.0345
R_1[a] (all data)	0.0442	0.0277
wR_2[b] (all data)	0.0819	0.0358
Flack parameter *x*	-0.01(5)	0.024(7)
$\Delta\rho_{max}/\Delta\rho_{min}$(eÅ^{-3})	1.5, -3.72	0.95, -0.78

Table S2. Atom coordinates and equivalent isotropic displacement parameters of **1** and **2**.

Atom	***x***	***y***	***z***	*U*eq(Å^2)
		1		
Ba(1)	0.25097(4)	0.49786(3)	0.75942(16)	0.0138(4)
Ba(2)	0.2500	0.7500	0.75988(15)	0.0136(4)
Ba(3)	0.5000	0.5000	0.50782(15)	0.0137(4)
Sn(1)	0.43053(5)	0.62505(6)	0.29797(6)	0.0117(2)
Sn(2)	0.38739(4)	0.62463(5)	0.75853(5)	0.0114(2)

Mn(1)	0.61106(10)	0.62404(13)	0.25565(16)	0.0182(4)
Mn(2)	0.32450(10)	0.62458(13)	0.47421(15)	0.0174(4)
S(1)	0.29523(18)	0.6244(4)	0.6531(2)	0.0125(8)
S(2)	0.53004(15)	0.6242(4)	0.3822(3)	0.0154(8)
S(3)	0.3767(2)	0.5410(4)	0.3762(5)	0.0137(16)
S(4)	0.3770(2)	0.7088(4)	0.3778(5)	0.0144(16)
S(5)	0.47091(15)	0.6238(3)	0.6399(2)	0.0149(7)
S(6)	0.3784(3)	0.7089(4)	0.8764(5)	0.0149(16)
S(7)	0.3770(2)	0.5421(4)	0.8792(5)	0.0141(16)
S(8)	0.45434(16)	0.6264(3)	0.1199(2)	0.0136(6)
		2		
Ba(1)	0.0000	0.0000	0.95449(17)	0.0137(3)
Ba(2)	0.0000	0.0000	0.44414(19)	0.0137(3)
Ba(3)	0.99668(3)	0.25165(2)	0.44885(19)	0.0137(3)
Ge(1)	0.06697(4)	0.12527(4)	0.16171(6)	0.01019(18)
Ge(2)	0.86070(4)	0.12490(6)	0.45354(7)	0.01025(17)
Cd(1)	0.88884(3)	0.12388(5)	0.20489(5)	0.02086(16)
Cd(2)	0.92356(4)	0.12524(5)	0.73370(5)	0.02052(17)
S(1)	0.11794(2)	0.04328(16)	0.1005(4)	0.0141(9)
S(2)	0.11790(16)	0.20622(11)	0.0987(4)	0.0137(9)
S(3)	0.97509(9)	0.12498(17)	0.07757(16)	0.0137(5)
S(4)	0.04270(9)	0.1265(3)	0.32891(16)	0.0141(5)
S(5)	0.8643(2)	0.04314(16)	0.3486(4)	0.0137(9)
S(6)	0.8648(2)	0.20558(16)	0.3464(4)	0.0147(9)
S(7)	0.94976(9)	0.12467(15)	0.54662(17)	0.0119(4)
S(8)	0.78470(9)	0.1263(3)	0.56984(17)	0.0140(5)

Table S3. The calculated $\triangle H$ and $\triangle R$ of asymmetric tetrahedral units, and formal oxidation state (V) and bond valence sum (S) of their central cations in **1** and **2**.

	V	*S*	*ΔH*	*ΔR*
		1		
$Sn(1)S_4$	4	4.09	0.0011	0.0003
$Sn(2)S_4$	4	4.06	0.0013	0.0003
$Mn(1)S_4$	2	2.06	0.0096	0.0024
$Mn(2)S_4$	2	2.05	0.0074	0.0018
		2		
$Ge(1)S_4$	4	3.99	0.0008	0.0002
$Ge(2)S_4$	4	3.96	0.0012	0.0003
$Cd(1)S_4$	2	2.04	0.0217	0.0053
$Cd(2)S_4$	2	2.02	0.0227	0.0055

Table S4. LIDTs of **1, 2** and Reference AGS with pulse width (τp) of 10 ns.

	damage energy (mJ)	spot area (cm^2)	damage threshold (MW cm^{-2})
1	61	0.196	31.067
2	78	0.196	39.7251
AGS	6	0.196	3.056

Table S5. The calculated Mulliken bond populations of chemical bonds in **1** and **2**.

			1		
Bond	distance	population	Bond	distance	population
Mn(1)-S(2)	2.397(4)	0.44	Ba(1)-S(2)	3.230(7)	0.12
Mn(1)-S(6)	2.495(8)	0.35	Ba(1)-S(1)	3.229(7)	0.12
Mn(1)-S(7)	2.481(8)	0.35	Ba(1)-S(5)	3.248(6)	0.12
Mn(1)-S(8)	2.498(4)	0.33	Ba(1)-S(4)	3.248(6)	0.12
Mn(2)-S(1)	2.406(4)	0.46	Ba(1)-S(3)	3.253(6)	0.12
Mn(2)-S(5)	2.486(4)	0.35	Ba(1)-S(8)	3.252(6)	0.11
Mn(2)-S(3)	2.491(7)	0.35	Ba(1)-S(7)	3.274(6)	0.12
Mn(2)-S(4)	2.494(7)	0.35	Ba(1)-S(6)	3.292(6)	0.11

Sn(1)-S(8)	2.367(3)	0.60	Ba(2)-S(1)	3.219(7)	0.12
Sn(1)-S(3)	2.394(7)	0.64	Ba(2)-S(8)	3.256(6)	0.12
Sn(1)-S(4)	2.396(7)	0.64	Ba(2)-S(7)	3.277(6)	0.12
Sn(1)-S(2)	2.407(4)	0.57	Ba(2)-S(6)	3.278(6)	0.12
Sn(2)-S(5)	2.369(3)	0.58	Ba(3)-S(2)	3.226(7)	0.13
Sn(2)-S(7)	2.397(7)	0.64	Ba(3)-S(5)	3.257(6)	0.11
Sn(2)-S(6)	2.399(7)	0.64	Ba(3)-S(4)	3.274(6)	0.11
Sn(2)-S(1)	2.412(4)	0.56	Ba(3)-S(3)	3.283(6)	0.11
			2		
Cd(1)-S(3)	2.4537(15)	0.48	Ba(1)-S(8)	3.273	0.13
Cd(1)-S(5)	2.584(4)	0.37	Ba(1)-S(1)	3.266	0.12
Cd(1)-S(5)	2.591(3)	0.36	Ba(1)-S(3)	3.179	0.13
Cd(1)-S(4)$^{\#1}$	2.6044(14)	0.37	Ba(1)-S(2)	3.261	0.11
Cd(2)-S(7)	2.4562(17)	0.51	Ba(2)-S(5)	3.272	0.11
Cd(2)-S(2)$^{\#2}$	2.587(3)	0.36	Ba(2)-S(4)	3.245	0.12
Cd(2)-S(1)$^{\#2}$	2.599(3)	0.35	Ba(2)-S(7)	3.190	0.12
Cd(2)-S(8)$^{\#3}$	2.6096(15)	0.38	Ba(2)-S(6)	3.270	0.11
Ge(1)-S(4)	2.1995(17)	0.64	Ba(3)-S(1)	3.271	0.11
Ge(1)-S(2)	2.215(3)	0.67	Ba(3)-S(5)	3.298	0.10
Ge(1)-S(1)	2.226(3)	0.68	Ba(3)-S(4)	3.268	0.11
Ge(1)-S(3)	2.2320(14)	0.61	Ba(3)-S(6)	3.255	0.13
Ge(2)-S(8)	2.1975(17)	0.63	Ba(3)-S(8)	3.237	0.12
Ge(2)-S(5)	2.224(3)	0.67	Ba(3)-S(2)	3.234	0.13
Ge(2)-S(5)	2.225(3)	0.67	Ba(3)-S(3)	3.198	0.11
Ge(2)-S(7)	2.2383(14)	0.59	Ba(3)-S(7)	3.185	0.13

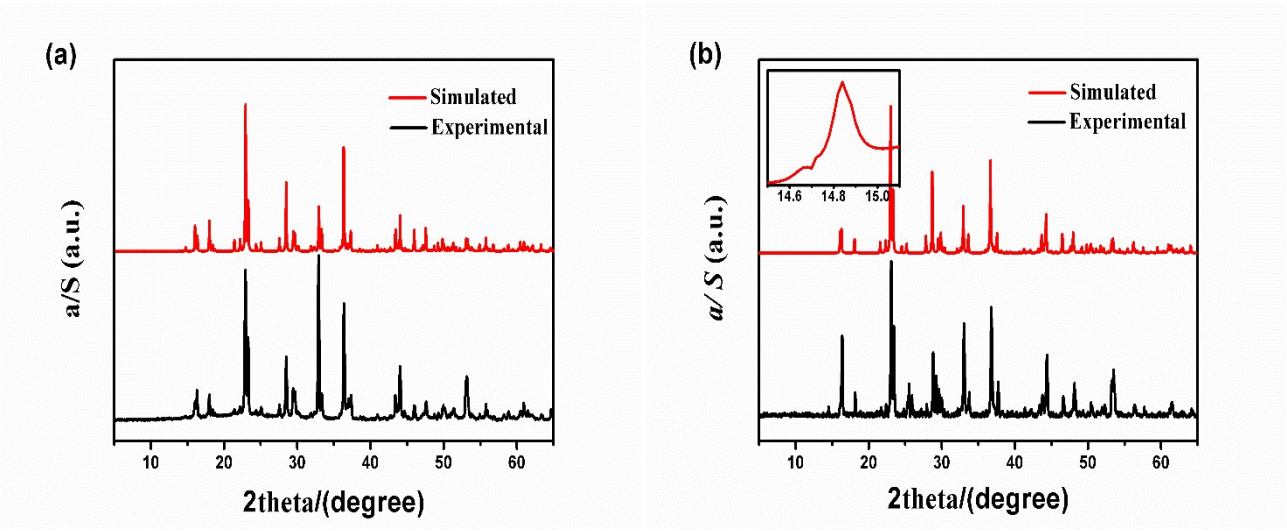

Figure S1. Experimental and simulated powder X-ray diffraction patterns of **1** (a) and **2** (b). Intensities of some peaks on the experimental patterns don't match those on the simulated ones because of the effect of preferred orientation.

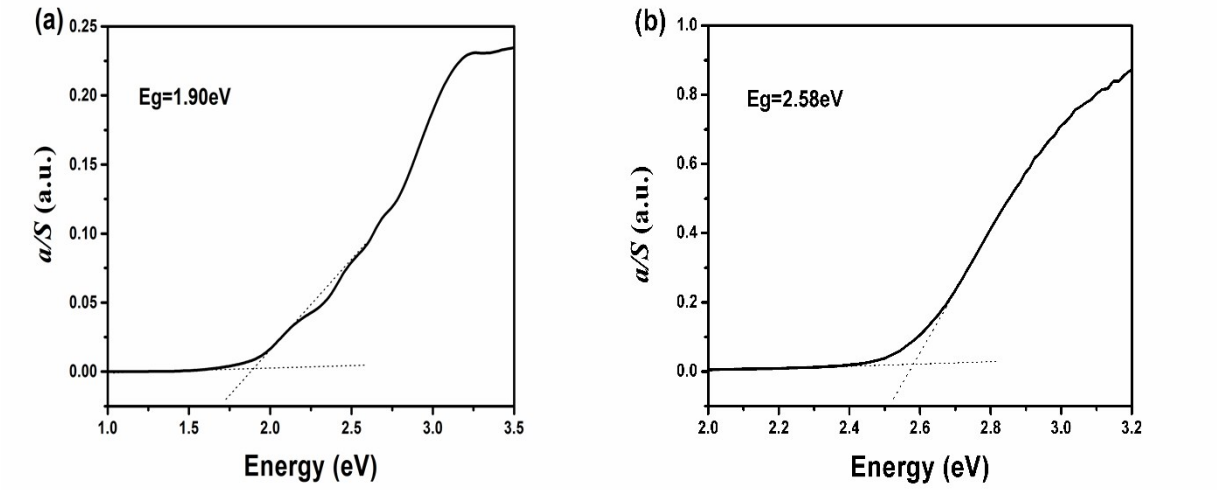

Figure S2. UV – Vis diffuse reflectance spectra of **1** (a) and **2** (b). The fluctuations around 2.2 eV in (a) are due to the *d-d* transitions of Mn^{2+}.

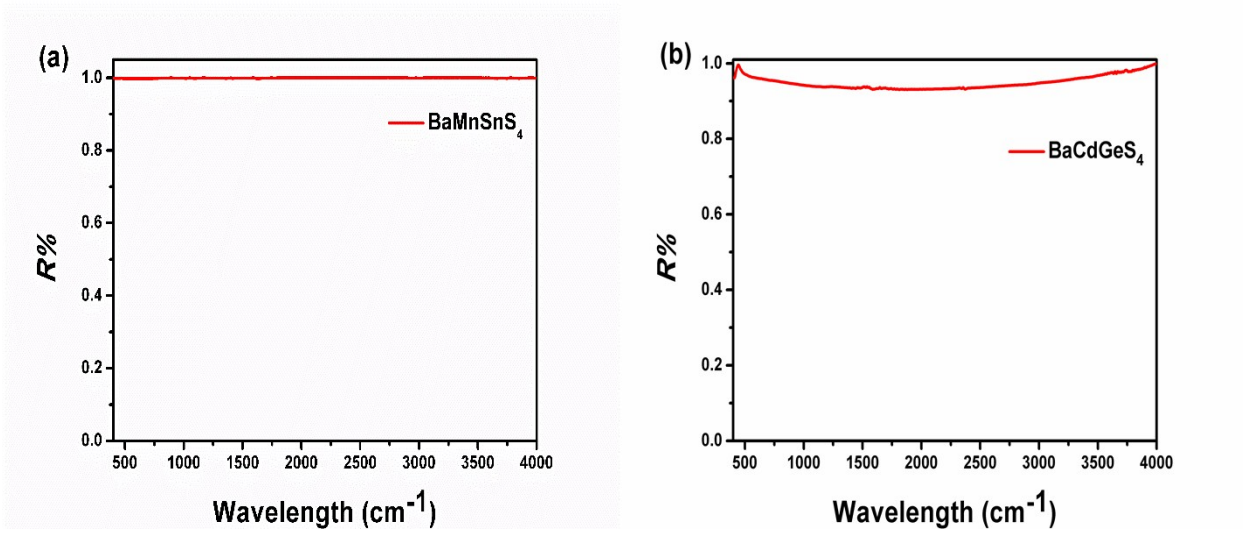

Figure S3. IR spectra of **1** (a) and **2** (b).

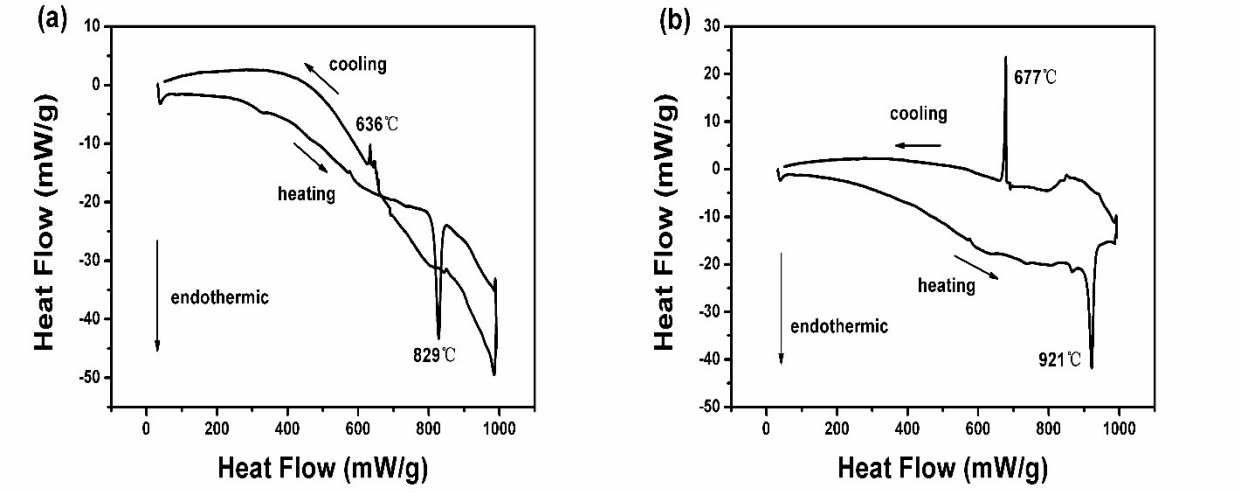

Figure S4. DSC curves of **1** (a) and **2** (b).

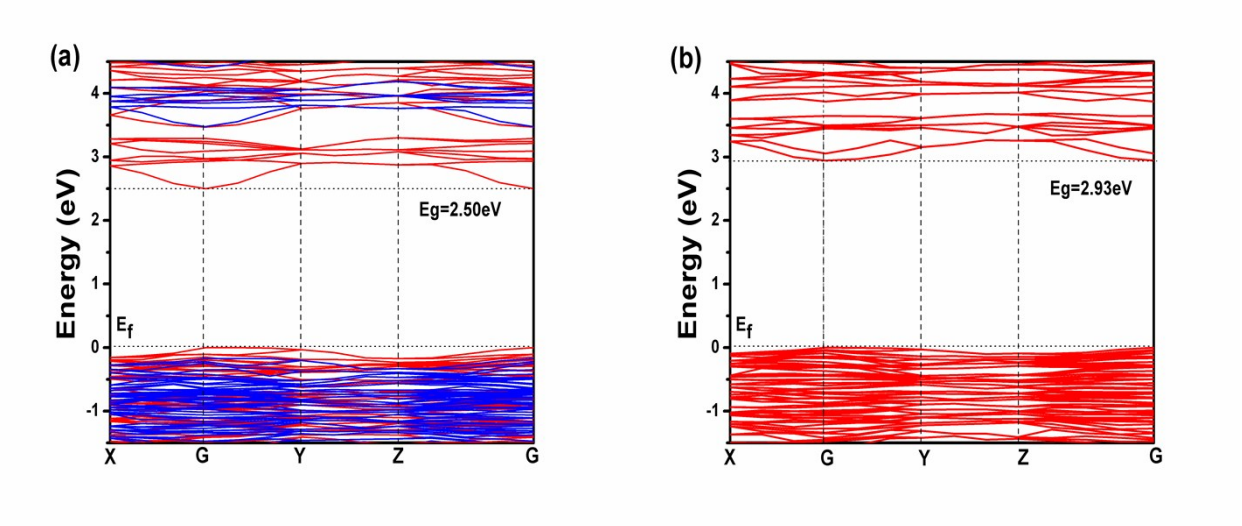

Figure S5. Band structures of **1** (a) and **2** (b). For compound **1**, band structures of up-spin (red line) and down-spin (blue line) for the ferromagnetic state are shown. The Fermi level is set at 0 eV for all the band structures.

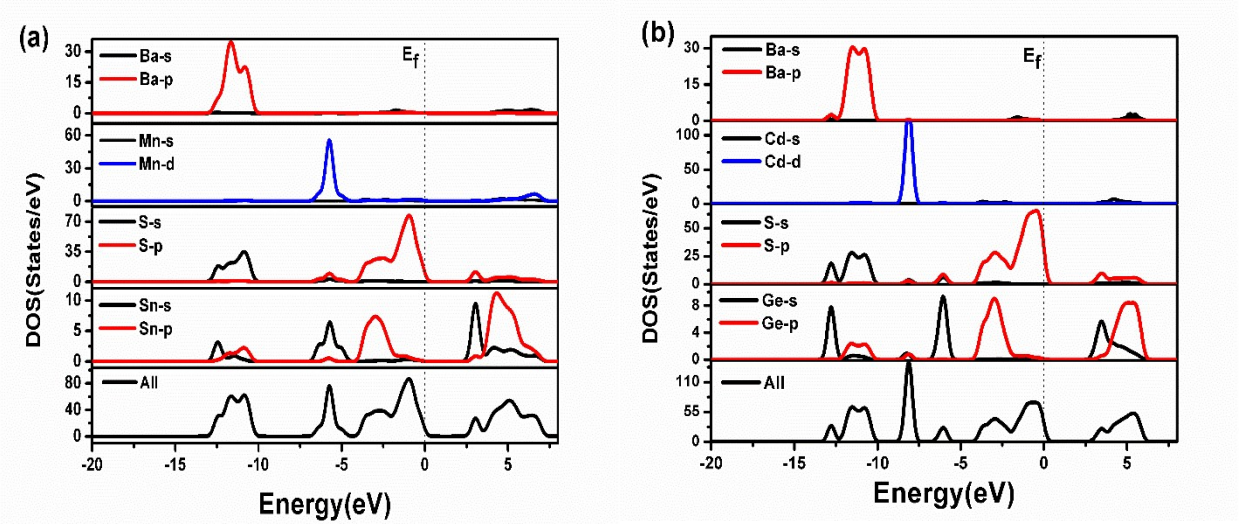

Figure S6. Total and partial DOSs of **1** (a) and **2** (b). The Fermi level is set at 0 eV for all the DOS.

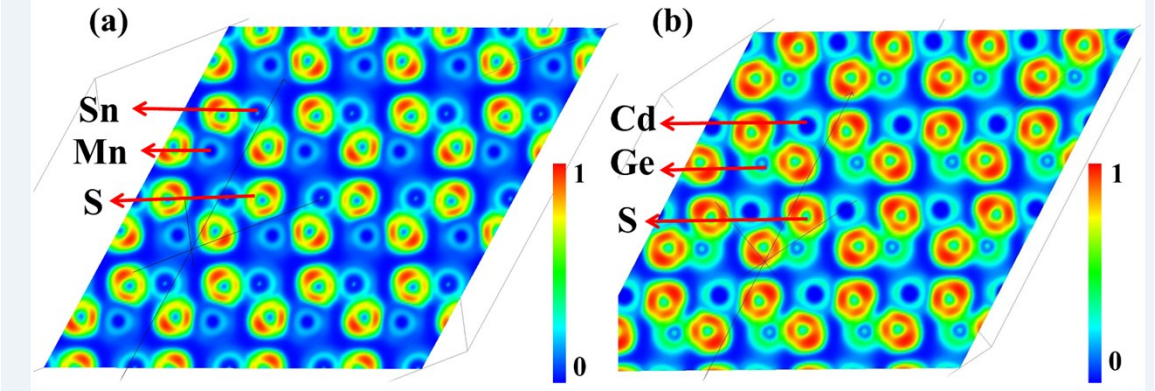

Figure S7. Electron localization function map of **1** (a) and **2** (b) at (010) plane cutting through the $(MnSnS_4)^{2-}$ layer in **1** and $(CdGeS_4)^{2-}$ layer in **2**.

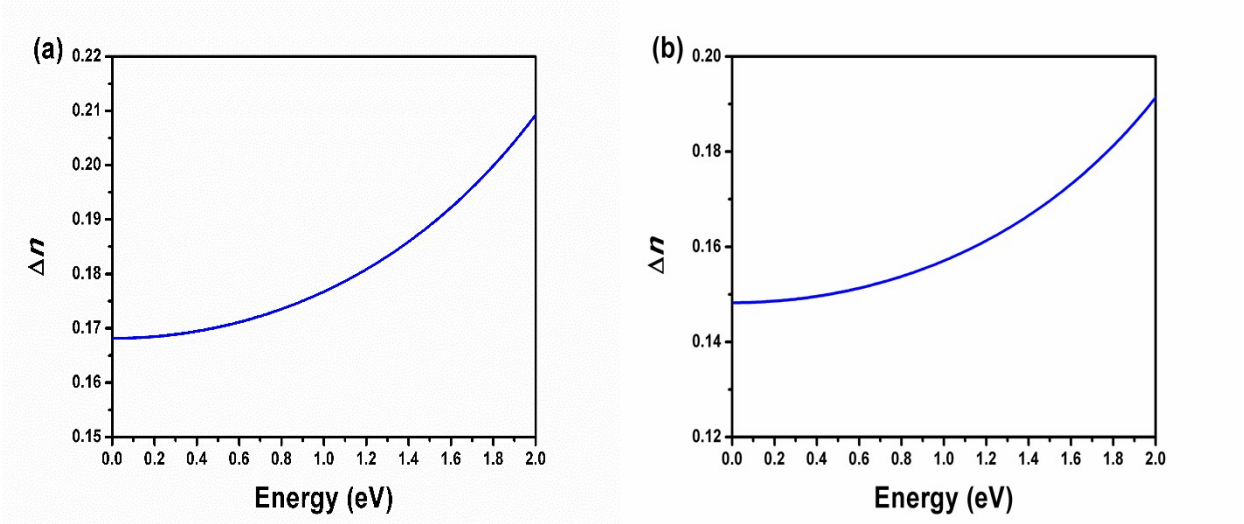

Figure S8. Calculated birefringence Δ*n* of **1** (a) and **2** (b).

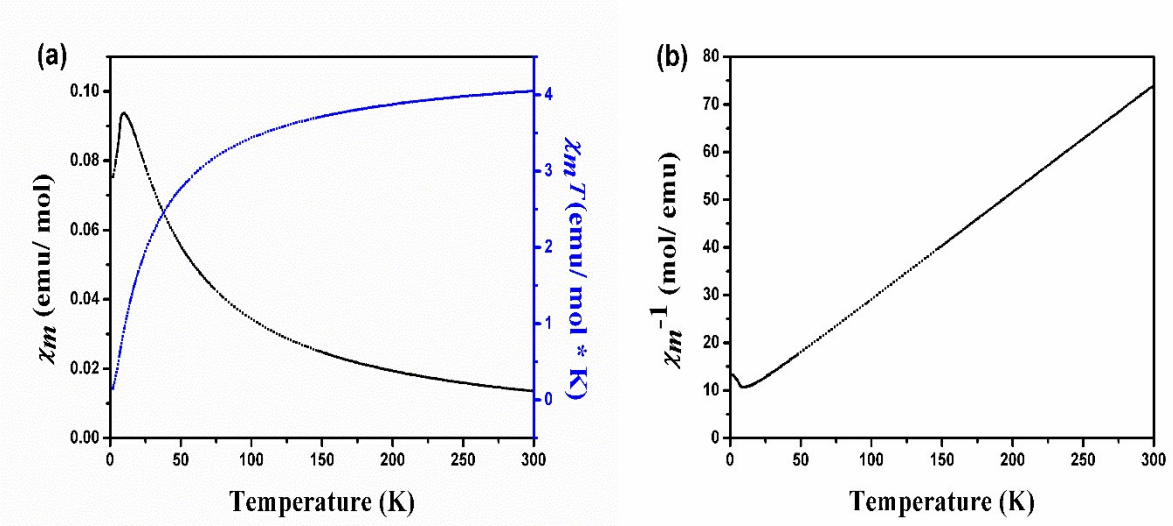

Figure S9. (a) Variable-temperature χ_m (left) and $\chi_m T$ (right) curves of **1**. (b) Variable-temperature $1/\chi_m$ curve of **1**.

3. References

(1) CrystalClear, version 1.3.5; Rigaku Corp.: Tokyo, **2002**.

(2) Sheldrick, G. M. SHELXS-97: program for X-ray crystal structure solution; University of Göttingen: Göttingen, Germany, **1997**.

(3) A. L. Spek, PLATON, A Multipurpose Crystallographic Tool, Utrecht University, Utrecht, The Netherlands, **2005**.

(4) Korum, G. Reflectance Spectroscopy; Springer: New York, **1969**.

(5) Kurtz, S.; Perry, T. A Powder Technique for the Evaluation of Nonlinear Optical Materials. *J. Appl. Phys.* **1968**, 39, 3798-3813.

(6) Zhang, M. J.; Jiang, X. M.; Zhou, L. J.; Guo, G. C. Two phases of Ga_2S_3: promising infrared second-order nonlinear optical materials with very high laser induced damage thresholds. *J. Mater. Chem. C.* **2013**, 1, 4754-4760.

(7) Lalik, E. Shannon information as a measure of distortion in coordination polyhedral. *J. Appl. Cryst.* **2005**, 38**,** 152-157.

(8) I. D. Brown, (2002). The Chemical Bond in Inorganic Chemistry: The Bond Valence Model. Oxford University Press.

(9) https://www.iucr.org/resources/data/datasets/bond valence-parameters

(10) Brown, I. D. On measuring the size of distortions in coordination polyhedral. *Acta Cryst.* **2006**, B62**,** 692-694.

(11) Payne, M. C.; Teter, M. P.; Allan, D. C.; Arias, T. A.; Joannopoulos, J. D.; Iterative minimization techniques for ab initio total-energy calculations: molecular dynamics and conjugate gradients. *Rev. Mod. Phys.* **1992**, 64, 1045-1097.

(12) Perdew, J. P.; Chevary, J. A.; Vosko, S. H.; Jackson, K. A.; Pederson, M. R.; Singh, D. J.; Fiolhais, C. Atoms, molecules, solids, and surfaces: Applications of the generalized gradient approximation for exchange and correlation. *Phys. Rev. B.* **1992**, 46**,** 6671-6687.

(13) Hamann, D. R.; Schlüter, M.; Chiang. C. Norm-Conserving Pseudopotentials. *Phys. Rev. Lett.* **1979**, 43**,** 1494-1497.

(14) (a) Gonze, X. Perturbation expansion of variational principles at arbitrary order. *Phys. Rev. A.* **1995**, 52**,** 1086-1095. (b) Gonze, X. Adiabatic density-functional perturbation theory. *Phys. Rev. A.* **1995**, 52**,** 1096-1114. (c) Gonze, X. First-principles responses of solids to atomic displacements and homogeneous electric fields: Implementation of a conjugate-gradient algorithm *Phys. Rev. B.* **1997**, 55**,** 10337-10354. (d) Gonze, X.; Lee, C.

Dynamical matrices, Born effective charges, dielectric permittivity tensors, and interatomic force constants from density-functional perturbation theory. *Phys. Rev. B.* **1997**, 55**,** 10355-10368. (e) Baroni, S.; Gironcoli, S.; Corso, D, A.; Giannozzi, P. 10.1103/RevModPhys.73.515. *Rev. Mod. Phys.* **2001**, 73**,** 515-562.

(15) Sharma, S.; Draxl, C. A. Second-Harmonic Optical Response from First Principles *Phys. Scripta. Vol.* **2004**, T109, 128-134.

(16) Yu, P.; Zhou, L. J.; Chen, L. Noncentrosymmetric Inorganic Open-Framework Chalcohalides with Strong Middle IR SHG and Red Emission: $Ba_3AGa_5Se_{10}Cl_2$ (A = Cs, Rb, K). *J. Am. Chem. Soc.* **2012**, 134**,** 2227-2235.

(17) (a) Kresse, G.; Hafner. J. Ab initio molecular dynamics for liquid metals. *Phys. Rev. B* **1993**, 47, 558−561. (b) Kresse, G.; Hafner. J. Ab initio molecular-dynamics simulation of the liquid-metal-amorphous-semiconductor transition in germanium. *Phys. Rev. B* **1994**, 49, 14251−14269. (c) Kresse, G.; Furthmüller, J. Efficiency of ab-initio total energy calculations for metals and semiconductors using a plane-wave basis set. *Comput. Mat. Sci.* **1996**, 6, 15−50. (d) Kresse, G.; Furthmüller, J. Efficient iterative schemes for ab initio total-energy calculations using a plane-wave basis set. *Phys. Rev. B* **1996**, 54, 11169−11186.